energies

MDPI

Article

Identifying Reservoir Features via iSOR Response Behaviour

Jingyi Wang and Ian Gates *

Department of Chemical and Petroleum Engineering, University of Calgary, Calgary, AB T2N 1N4, Canada; jwang@ucalgary.ca

* Correspondence: ian.gates@ucalgary.ca

Abstract: To extract viscous bitumen from oil sands reservoirs, steam is injected into the formation to lower the bitumen's viscosity enabling sufficient mobility for its production to the surface. Steam-assisted gravity drainage (SAGD) is the preferred process for Athabasca oil sands reservoirs but its performance suffers in heterogeneous reservoirs leading to an elevated steam-to-oil ratio (SOR) above that which would be observed in a clean oil sands reservoir. This implies that the SOR could be used as a signature to understand the nature of heterogeneities or other features in reservoirs. In the research reported here, the use of the SOR as a signal to provide information on the heterogeneity of the reservoir is explored. The analysis conducted on prototypical reservoirs reveals that the instantaneous SOR (iSOR) can be used to identify reservoir features. The results show that the iSOR profile exhibits specific signatures that can be used to identify when the steam chamber reaches the top of the formation, a lean zone, a top gas zone, and shale layers.

Keywords: steam-assisted gravity drainage (SAGD); steam-to-oil ratio (SOR); process performance; thermal efficiency

Citation: Wang, J.; Gates, I. Identifying Reservoir Features via iSOR Response Behaviour. *Energies* **2021**, *14*, 427. https://doi.org/10.3390/en14020427

Received: 9 December 2020
Accepted: 13 January 2021
Published: 14 January 2021

1. Introduction

The method of choice for producing deep bitumen-bearing oil sands reservoirs that cannot be mined is the steam-assisted gravity drainage (SAGD) process [1–3], displayed in cross-section in Figure 1. The key challenge of these reservoirs is that the oil is its viscosity with values in the hundreds of thousands to millions of cP at the original reservoir temperature [1–4]. In the SAGD process, steam is injected into the reservoir to heat the bitumen which consequently lowers its viscosity. At roughly 200 °C, the viscosity of bitumen is typically lower than 20 cP making it sufficiently mobile to be drained under gravity and be produced to surface [3,5]. One of the key challenges faced by SAGD is its emissions intensity—the fuel combusted to generate steam creates greenhouse gas emissions to the atmosphere [6]. Another challenge is its economics—the operating cost of steam generation (fuel costs) and other operating costs together with the revenues obtained for bitumen which is generally priced at a discount relative to sweet conventional oil due to its viscosity, sulphur content, and total acid number [7]. The emissions and economic intensities of SAGD are reflected by the steam-to-oil ratio (SOR)—the higher the steam per unit volume bitumen produced, the greater are the emissions as well as costs per unit volume bitumen produced. Thus, there is a strong motivation for oil sands operators to lower the SOR as much as possible. However, other factors may prevent an operator from reaching the theoretical SOR, roughly equal to 0.7 m^3/m^3 (where steam is expressed as cold water equivalent) in a SAGD operation [6].

Several authors have examined strategies to control the SOR of SAGD [8–19]. For example, Gates and Chakrabarty [8] used the SOR as a means to control the recovery process by using an automated optimization algorithm to determine a strategy for reducing the SOR of SAGD. Their results showed that the optimal strategy involved a sequence of injection pressure reductions as the process evolves to recover energy from the reservoir placed there earlier in the process. Edmunds and Chhina [20] studied a series of McMurray

reservoirs with pay thicknesses between 10 and 25 m and horizontal permeability between 3.5 and 7 Darcy. At various injection pressures, the economics of the SAGD operation was found to be more sensitive to the SOR than the oil production rate itself. If the natural gas price is high, then the reduction of the SOR becomes critical for the project [8]. Gates et al. [9] controlled the SAGD injection pressure in a top gas reservoir to ensure that the SOR was managed. Bao [10] studied a vertical and horizontal well combination SAGD field case. The study used proportional-integral-derivative (PID) control to allocate steam between wells dynamically. The setpoint for the control algorithm is the temperature observation data within the field. With PID control, optimized steam injection strategy achieved more uniform steam chamber growth and lower SOR. In another example, Guo et al. [11] examined the use of the iSOR as a setpoint variable in a feedback control strategy to reduce the overall SOR of a pad of SAGD well pairs. They showed that using the iSOR in the control strategy could lower the cumulative SOR (cSOR) by up to 16% (the cSOR is the ratio of the cumulative steam injected up to a point of time and the cumulative oil produced up to that point of time). As yet, despite the results from the literature, substantial improvement of SAGD performance remains elusive.

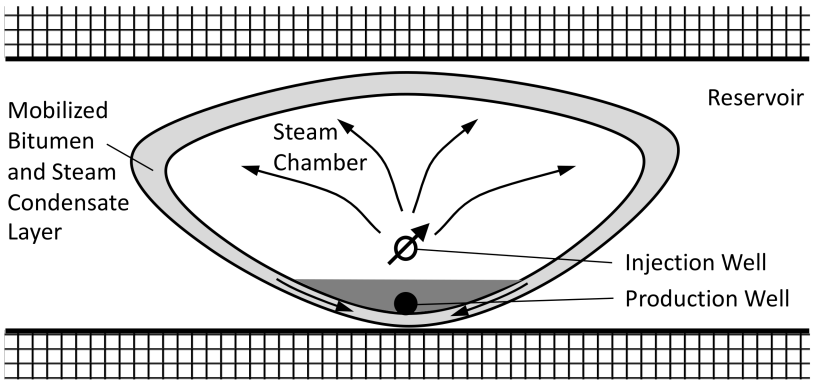

Figure 1. Cross-sectional view of steam-assisted gravity drainage (SAGD) process. Steam injected into the reservoir through the top well flows to the outer edge of the steam chamber and condenses there releasing its latent heat when it comes into contact with the cooler oil sands there. The heated bitumen, given the increase of its mobility, drains under gravity to the base of the steam chamber where the production well is located.

Several factors that interfere with the achievement of an ideal SOR are listed as follows:

(1) Non-ideal well trajectories (undulations can interfere with ideal conformance of steam injection and fluid production along a SAGD well pair) [15,16],
(2) Heterogeneity of the formation (e.g., porosity, permeability, phase saturations, and rock type) along the well pair (also leading to non-ideal steam conformance along the well pair) [13–15],
(3) Non-uniform pressure along the wells (leading to non-uniform injection into the reservoir or fluid production from the reservoir) [15,16],
(4) Heat losses to non-productive rock (the steam's latent heat not being delivered to productive oil sands zones)—this cannot be avoided after the steam chamber reaches the top of the formation [11–14,21],
(5) Merging of non-uniform steam chambers at one or more points along two adjacent well pairs can lead to reinforcement of non-uniform conformance along one or both well pairs,
(6) Presence of non-permeable reservoir rock within the oil sands formation (shale layers interfere with steam ascension and oil and condensate drainage) [12–14,22], and
(7) Larger scale features associated with the oil sands reservoir including top water and gas zones and bottom water zones (can become pressure sinks or sources leading to steam loss or water ingress) [9,11,17].

Given that the above features adversely affect the SOR, it is reasonable to think that the SOR could be used to detect the presence of one or more of the features. A better understanding of the SOR response as a means to understand the features adversely affecting the process may yield an understanding of how to adjust the operation to improve the performance of the recovery process. In this work, a reservoir simulation model is used to examine the response of the instantaneous steam-to-oil ratio (iSOR) to different features within the reservoir. The iSOR is the ratio of the amount of steam injected in a single day to the amount of bitumen produced in that day. Despite the different time scales for steam injection and bitumen mobilization, drainage, and production, the iSOR will be used here because it is an established measure of process performance that SAGD operators monitor during the process. However, it has not been used before as a signal for decoding how the reservoir is responding to the injected steam.

2. Reservoir Simulation Model

Here, the base case reservoir model (Case 1) is a relatively simple two-dimensional domain, as shown in Figure 2a, with reservoir characteristics typical of that of an Athabasca oil sands reservoir, as listed in Table 1. In the vertical direction, there are ten 1 m grid blocks plus two hundred and thirty-three 0.1 m grid blocks for a total reservoir thickness of 33 m. There are one hundred and two 2 m grid blocks in the cross-well direction for a total reservoir width of 204 m. In the down well direction there is a single grid block with length 100 m. The SAGD well pair is positioned at the center of the reservoir domain with the production well 5 m above the base of the reservoir and the injection well placed 5 m above the production well. At the side walls of the domain, the boundaries are symmetry boundaries. At the top and bottom boundaries, heat transfer is allowed according to Vinsome and Westerveld's heat loss model [23] but no flow is permitted.

There are three other cases that are variants of the base case model, described as follows. Cases 2a and 2b, displayed in Figure 2b, are the same as the base case except the top 5 and 8 m of the domains are lean zones (oil saturation in the lean zone is equal to 0.4 with the remainder being water), respectively. Cases 3a and 3b, shown in Figure 2c, have 5 and 8 m gas zones at the top of the reservoir (gas saturation equal to 0.8 with the remainder being oil), respectively. Cases 4a and 4b are presented in Figure 2d and are the same as the base case with a 0.5 m thick 20 and 40 m wide impermeable shale layer placed 11 m directly above the injection well, respectively.

Before SAGD, a steam circulation stage is modelled to establish thermal communication between the injection and production wells for three months. To model this pre-heating stage, the wells are treated as line heat sources for three months with production allowed at both wells to relieve the pressure due to thermal expansion of the fluids in the reservoir. At the end of the pre-heat stage, SAGD starts with injection of steam (95% quality, 4000 kPa, 250.3 °C) into the reservoir through the upper well and production of fluids through the lower well. The maximum steam production rate is constrained to 1.0 m^3/day CWE (cold water equivalent) to mimic steam trap control at the production well. To ensure that the results were independent of grid dimensions, the grid-blocks were halved in all three directions: the results from the original and finer grid block simulations showed less than 0.1% difference of the fluid injection and production profiles proving that the original grid was sufficiently refined.

The model's governing equations are the multiphase Darcy's law for the flow of each phase (oil, water, and gas), the material balance, and the energy balance, as summarized in Table 2. This set of coupled partial differential equations is solved by using the CMG thermal reservoir simulator STARS^{TM} [24]. This simulator uses the finite volume method to discretize the governing equations which are then solved by using Newton's method with an implicit time integrator to march through time. In each grid block at each time step, a phase equilibrium *K*-value compositional solver is utilized to partition the solution gas between the oil and gas phases at the grid block conditions.

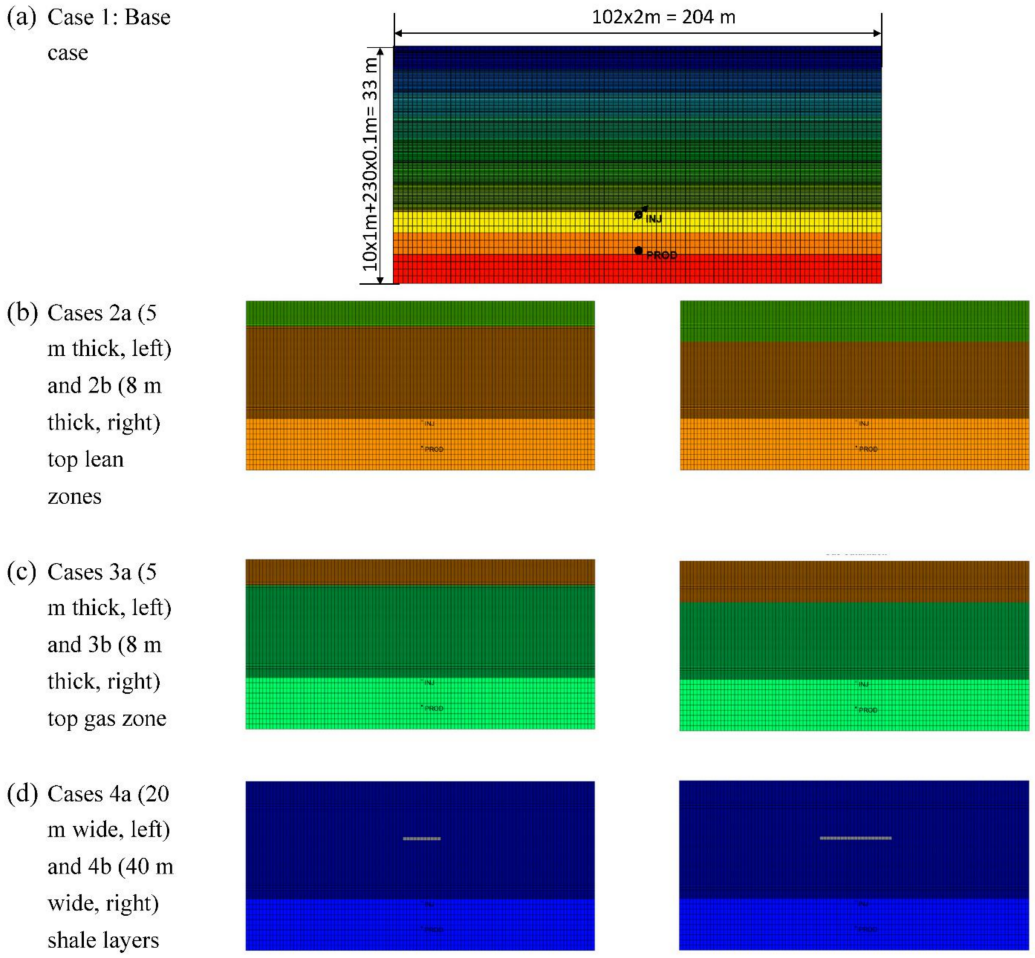

Figure 2. Reservoir simulation model cases (the images have been exaggerated in the vertical direction by 3 times).

Table 1. Oil sands reservoir properties.

Item	Value
Steam circulation (pre-heat) period, months	3
SAGD operation period, years	10
Initial reservoir temperature, °C	12
Initial reservoir pressure at depth 350 m, kPa	3000
Initial oil saturation	0.75
Porosity	0.3
Horizontal permeability, mD	3000
Vertical-to-horizontal permeability ratio	0.5
S_{orw}	0.2
S_{wc}	0.15
S_{org}	0.15
S_{gc}	0.05
k_{rwro}	0.1
k_{rocw}	0.992
k_{rogc}	0.992
$k_{rg(Sorg)}$	1.0

Table 1. *Cont.*

Item	Value
Reservoir rock and overburden/understrata heat capacity, kJ/m^3 °C [2]	2600
Reservoir rock and overburden/understrata thermal conductivity, kJ/m day °C [2]	660
Bitumen thermal conductivity, kJ/m day °C [2]	11.5
Water thermal conductivity $k_{TH(w)}$, kJ/m day °C [2]	53.5
Gas thermal conductivity $k_{TH(g)}$, kJ/m day °C [2]	5.0
Bitumen viscosity correlation, cP, T in °C $\ln(\ln(\mu + 0.7)) = A + Bln(T + 273.15) + C[ln(T + 273.15)]^2$	A = −9.1919 B = 7.3008 C = −0.917
Solution Gas to Oil Ratio, m^3/m^3	2
Methane *K*-value correlation, *K*-value = $\frac{k_{v1}}{P} e^{\frac{k_{v4}}{T+k_{v5}}}$ [24]	k_{v1} = 5.4547 × 10^5 kPa k_{v4} = −879.84 °C k_{v5} = −265.99 °C

Table 2. Governing equations.

Item	Equation	
Multiphase flow in porous media (Darcy's law)	$u = -\frac{k_*}{\mu_*} \nabla \Phi_*$	
Potential	$\Phi = g(z - z_{datum}) + \int_{P_{datum}}^{P} \frac{dP}{\rho}$	
Material balance (equation of flow)	$\nabla \cdot \left[\frac{R_{sw} k_w}{\mu_w B_w} (\nabla P_w - \rho_w g \nabla z) + \frac{R_{so} k_o}{\mu_o B_o} (\nabla P_o - \rho_o g \nabla z) + \frac{k_g}{\mu_g B_g} \nabla P_g - \rho_g g \nabla z \right) =$ $\frac{\partial}{\partial t} \left[\varphi \left(\frac{R_{so} S_o}{B_o} + \frac{R_{sw} S_w}{B_w} + \frac{S_g}{B_g} \right) \right] + \frac{R_{so} q_o}{B_o} + \frac{q_{fg}}{B_g}$	
Conductive heat transfer	$q = -k_{th} \nabla T$	
Energy balance	$\frac{\partial}{\partial x}(-k_{th} \frac{\partial T}{\partial x} + \sum_{i=1}^{n_p} u_{i,x} \rho_i h_i) + \frac{\partial}{\partial y}(-k_{th} \frac{\partial T}{\partial y} + \sum_{i=1}^{n_p} u_{i,y} \rho_i h_i) + \frac{\partial}{\partial z}(-k_{th} \frac{\partial T}{\partial x}$ $+ \sum_{i=1}^{n_p} u_{i,z} \rho_i [h_i + gz/(Jg_c)]) =$ $\frac{\partial}{\partial t} \left[(1 - \phi) M_r \left(T - T_{ref} \right) + \phi \left(S_w \rho_w U_w + S_o \rho_o U_o + S_g \rho_g U_g \right) \right] + Q$	
Symbol definitions	Subscripts w, o, and g refer to the water, oil, and gas phases, respectively	
	u_*	velocity of phase
	k_*	effective permeability tensor of phase
	μ	viscosity
	$\nabla \Phi_*$	potential gradient of phase
	g	acceleration due to gravity
	ρ	density
	z	elevation above datum location
	R_{sw}, R_{so}	solution-gas ratios in oil or water phases, respectively
	k_o, k_w, k_g	effective permeabilities of oil, water and gas, respectively
	B_o, B_w, B_g	formation volume factors for oil, water, and gas, respectively
	q	heat transfer flux
	k_{th}	thermal conductivity tensor
	T	temperature
	h_i	enthalpy of each phase
	M_r	volumetric heat capacity of reservoir solids
	U_*	specific internal energy of each phase
	Q	energy input per unit volume

3. Results and Discussion

3.1. Case 1: Base Case

Figure 3 displays the overall results of the reservoir simulation including the cumulative steam injected, cumulative water produced, cumulative oil produced, and injection and production well bottomhole pressures. The cumulative bitumen produced after 10 years of operation is equal to about 55,000 m^3 (for a 100 m long domain; if taken to typical SAGD well pair length of 800 m, this would be 440,000 m^3 or 2.77 million barrels). The steam injection and oil rate profiles have the ramp up, plateau, and slow decline signature typical of that of a SAGD operation.

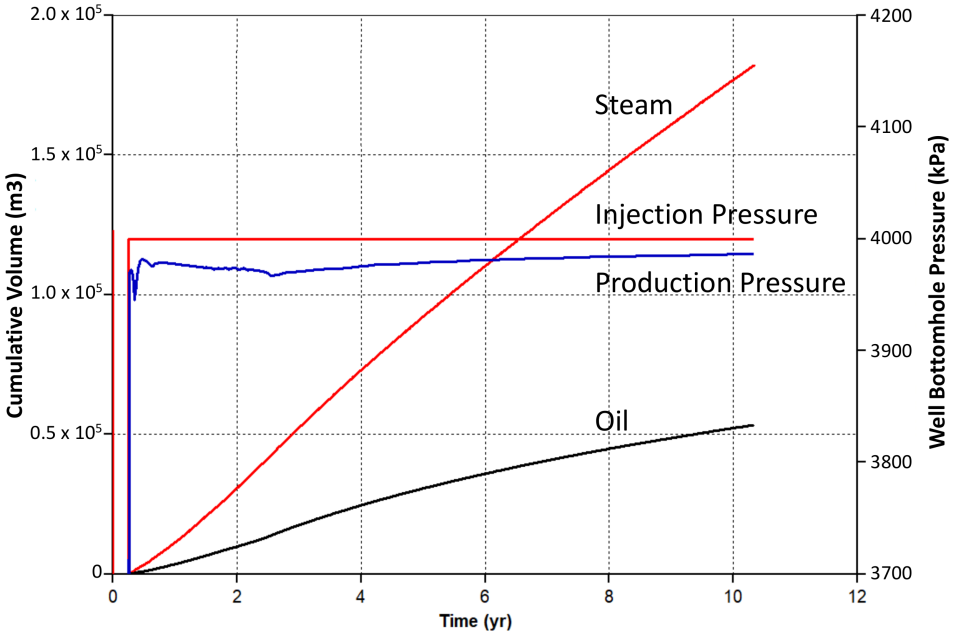

Figure 3. Performance of base case SAGD operation.

Figure 4 shows the iSOR, cSOR, and steam injection, water production, and oil production rates. The results are typical of that of SAGD operations in the Athabasca oil sands deposit with a minimum of about 3 m^3/m^3 rising to about 3.5 m^3/m^3 by the end of 10 years of operation. Since the cSOR is an integrated quantity (being cumulative volumes), its profile is smooth. On the other hand, the iSOR profile is relatively rough with an early stage plateau (on average) eventually reaching a minimum value where there is a distinct change of the slope after which, the iSOR then climbs through time. At Time A, the chamber has just started to rise within the reservoir and there are limited fluctuations of the iSOR profile. At Time B, the chamber has reached the top of the reservoir with a vertical shape where the steam is rising to the top of the formation, condensing there, and then draining downwards counter-current to the steam flow—the flows of the steam (gas phase) and liquid water condensate interfere with each other. The minimum value of the iSOR profile at Time C corresponds to the point of time where the 'thermal momentum' of the steam chamber has been established where the shape is now wider, the steam rises up the middle of the chamber, and the condensate largely drains down the sides of the chamber. At Time C, there is a distinct change of the slope of the iSOR profile. Beyond Time C, the steam chamber continues to extend laterally across the domain. Time C also corresponds to the point in time when the steam injection rate and bitumen production rate start to decline after the plateau stage of the process.

The iSOR signature shown in Figure 4 reveals that during the rising chamber stage, the iSOR has undulations but that it is relatively smooth. However, during the plateau stage where the chamber is establishing itself at the top of the reservoir, the iSOR becomes erratic; after it has fully established itself, it reaches its minimum value. Thereafter, after

the chamber starts to expand laterally, the iSOR starts to climb in a nearly linear manner. The results suggest that despite the time scales between injection and flow to the edge and top of the chamber and bitumen mobilization, drainage, and production, the iSOR is responding to what the steam chamber is encountering within the reservoir and that it can be used as a signal to understand the evolution of the process.

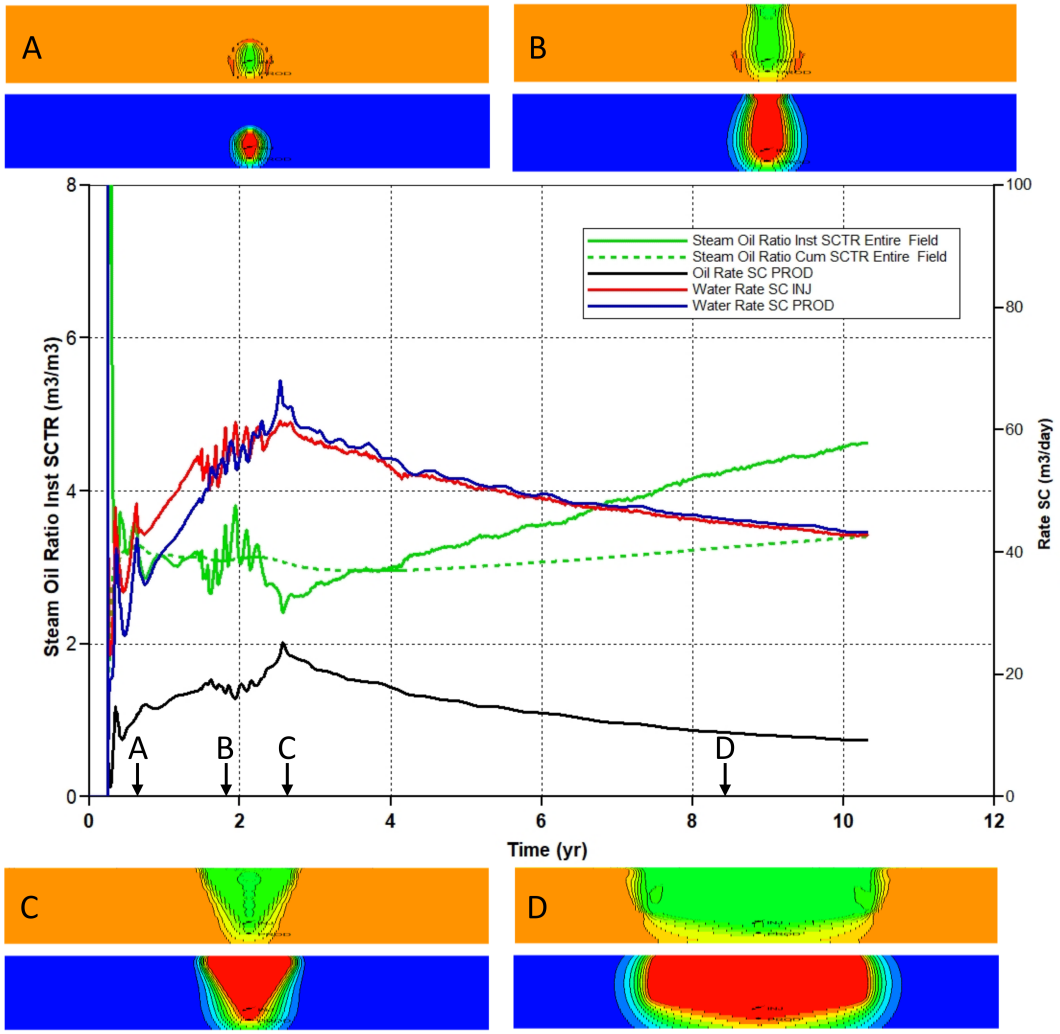

Figure 4. iSOR, cSOR, and rate profiles of base case SAGD operation. Top images of reservoir are the oil saturation (brown = 0.75, green = ~0.22) and bottom images are the temperature profile (blue = 12 °C, red = 250 °C). The image labels (**A**–**D**) correspond to the times (**A**–**D**) in the plot.

Figure 5 displays the evolution of the iSOR and the temperature and phase (oil, water, and gas) saturations in the top-most grid block of the reservoir directly above the SAGD well pair. The results show that the thermal front reaches the top of the reservoir after about 14 months of SAGD operation as reflected by the rise of the temperature. First, the temperature front reaches the top of the reservoir and the top most block starts to heat up. After the temperature starts to rise, the oil saturation drops from its initial value of 0.75 to ~0.22 as it drains from the top of the reservoir whereas the gas saturation rises from zero to about 0.45 and then more slowly climbs to over 0.6 after ten years of SAGD operation. The water saturation in the top-most grid block initially drops when the chamber reaches the top of the reservoir and then rises sharply to a peak value of ~0.35 and then drops slowly to about 0.25 after ten years of SAGD operation. As a consequence of the grid block below (with its relatively high gas saturation) and the mobilization of the bitumen, the bitumen in the top-most block drains and more steam enters the block (the replacement

mechanism of SAGD) which in turn, further accelerates the heating of the grid block leading to the rapid temperature rise in the topmost grid block. During the drainage period when the oil saturation drops from the original oil saturation to ~0.22, the iSOR is fairly smooth. However, after the oil saturation has reached its new value (close to the residual oil saturation), the iSOR becomes quite rough and fluctuates significantly with a downward trend until it reaches a minimum value. This signifies that the steam chamber has established itself at the top of the reservoir and has now started spreading laterally.

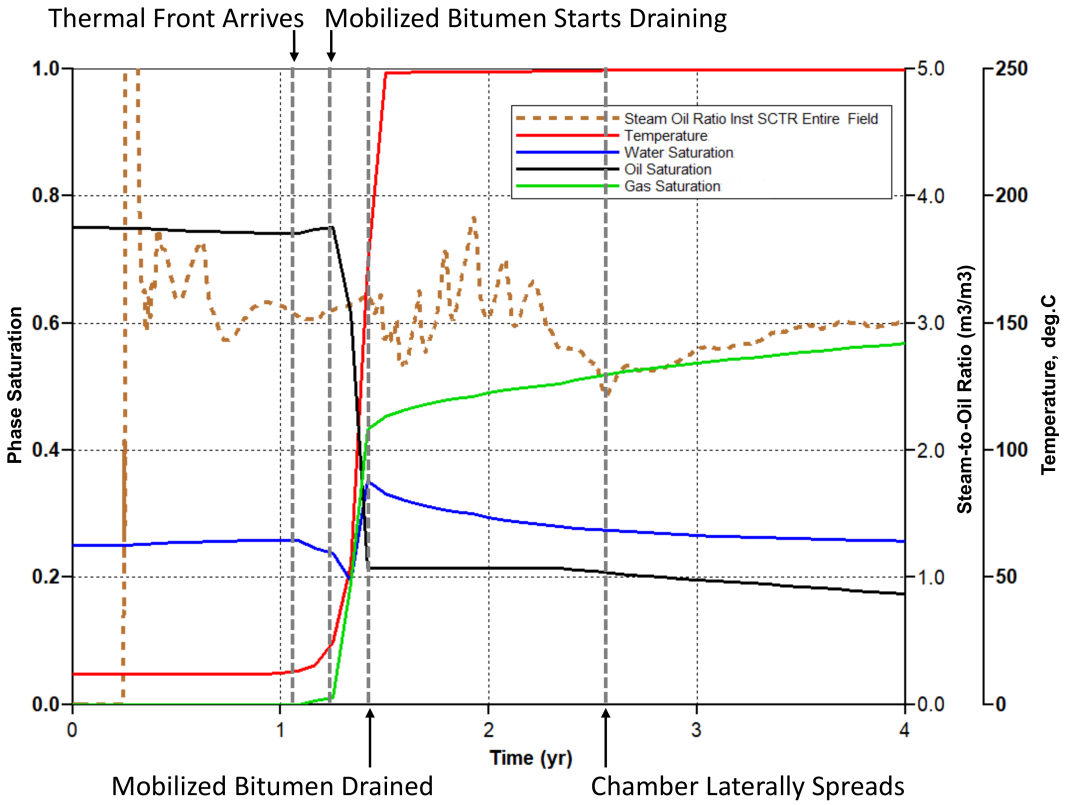

Figure 5. iSOR, temperature, and phase saturation profiles at topmost grid block above the SAGD well pair.

Figure 4 illustrates that the main cause of the iSOR response when the steam chamber reaches the top of the reservoir arises from the fluctuations of the steam rate. In the period when the chamber is more vertical in shape, as shown at Time B in Figure 4, the steam and water interfere with each other since the chamber is relatively narrow. The produced water fluctuations are aligned with the steam injection fluctuations. The steam is injected at constant pressure and when the steam reaches the top of the chamber and experiences the cold overburden, the steam condenses forming steam condensate. The condensate then has to drain from its location adjacent to the reservoir cap rock for new steam to replace it, which will subsequently condense and repeat the drainage and steam replacement process. Thus, a cyclic behaviour sets in where steam flows into the space, it condenses, then drains, and then is replaced (condensation-drainage-replacement cycle) by new steam leading to the oscillatory steam rate required to maintain the pressure constant in the chamber. The oil rate responds counter to the steam injection rate due to relative permeability competition between oil and water that occurs at the production well. The time lag between the injection stimulus and oil production response may also contribute to this behaviour. The oil exhibits counter fluctuations of the oil rate with respect to the steam and produced water rates which accentuates the oscillations of the iSOR. The oil peak leads to the minimum of the iSOR. The bitumen peak corresponds to approximately 1 year after the steam chamber has reached the top of the reservoir—this speaks to the time scale for the steam to flow to the top and the bitumen to be mobilized and drained to the production well.

3.2. Case 2: Lean Zone

Figure 6 displays the steam injection rate, oil and water production rates, and iSOR and cSOR profiles for Case 2a where there is a 5 m thick low oil saturation (lean) zone at the top of the reservoir. In this case, prior to when the steam chamber reaches the bottom of the lean oil zone, the iSOR profile is similar to the base case profile. After the chamber reaches the lean zone, the iSOR profile responds with a rapid increase which then reaches a peak value than then drops, in a relatively smooth manner, to a minimum value with a distinct change of the slope. Beyond this point, after the 'thermal momentum' of the steam chamber is established at the top of the reservoir, the iSOR rises nearly linearly. A comparison of the base case and Case 2a reveals that the iSOR response arises from two causes: 1. the oil rate is lower during the period at which the steam chamber has reached the top of the chamber and 2. the lower oil saturation and higher water saturation in the top zone softens the response of the condensation-drainage-replacement cycles of steam when the steam chamber reaches the top of the reservoir. In combination with the base case, the results suggest that a relative permeability effect between the condensate above and the steam below may lead to a stronger condensation-drainage-replacement cycle behaviour. In contrast, when the water saturation in the top zone is higher (as is the case in the lean zone), the interference of the steam on the water counter flow is less (due to the higher water saturation).

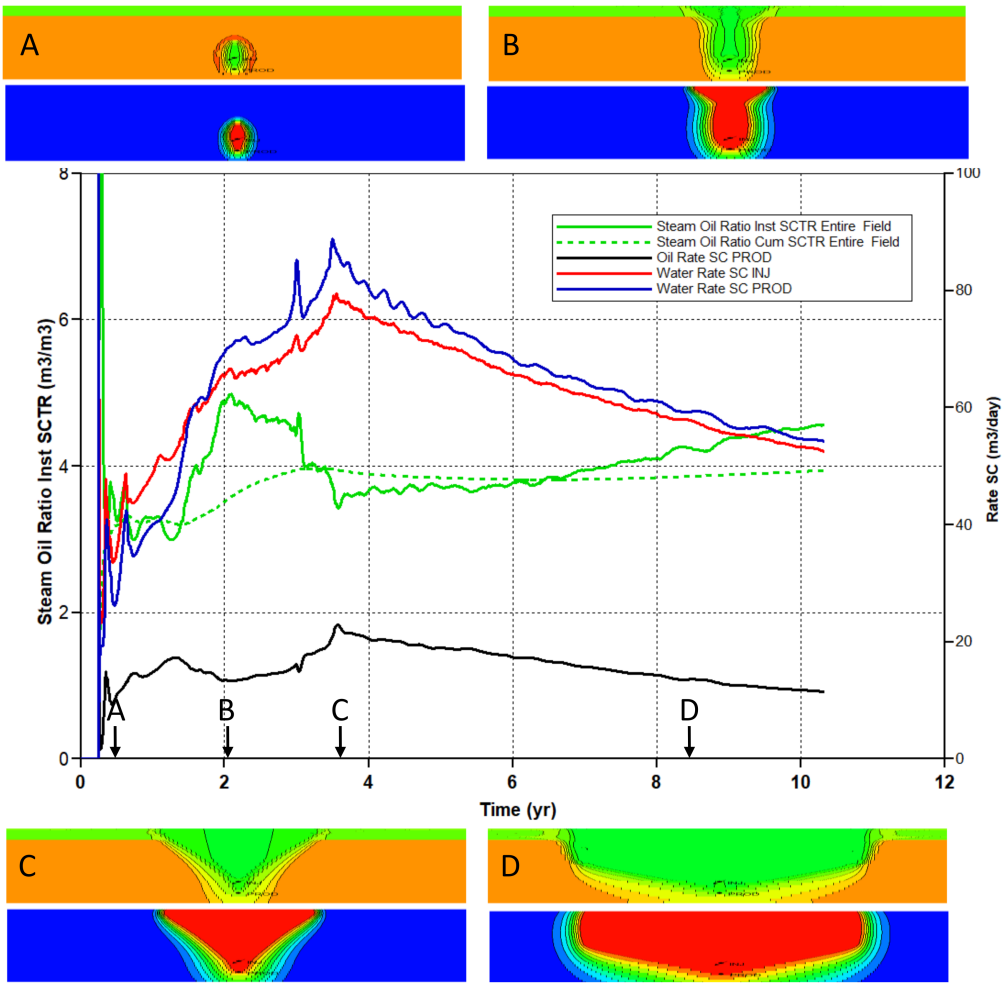

Figure 6. iSOR, cSOR, and rate profiles of SAGD operation with 5 m thick lean zone at the top of the reservoir. Top images of reservoir are the oil saturation (brown = 0.75, green = ~0.22) and bottom images are the temperature profile (blue = 12 °C, red = 250 °C). The image labels (**A**–**D**) correspond to the times (**A**–**D**) in the plot.

The results show that after 'thermal momentum' is established, there is a distinct change of the slope of the iSOR. One other observation of the iSOR response is that the minimum in its profile is delayed by just under 1 year when there is a lean zone at the top of the reservoir. Thus, the timing of the minimum of the iSOR also provides a signal that can be used to compare different well pairs providing insight on the relative natures of the top of the formations above each well pair.

Figure 7 compares the iSOR and cSOR profiles of the 5 and 8 m thick lean zone cases. The results show that the iSOR profiles' shape is similar, but the 5 m case has a broader shape with a higher peak value. The point of the minimum iSOR (where there is a distinct change of the slope) is delayed in the 5 m case relative to the 8 m case. The results also show that the thicker is the lean zone, the greater is the cSOR.

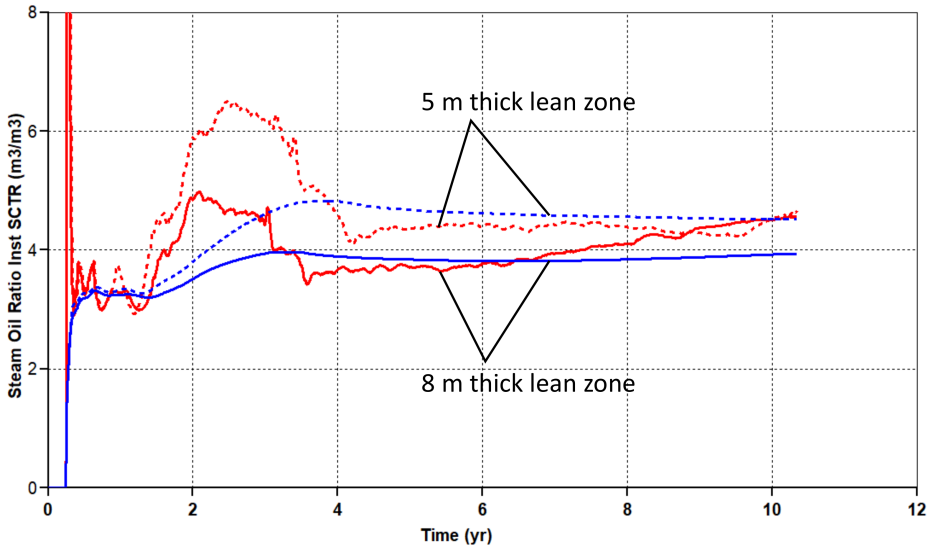

Figure 7. Comparison of iSOR (red) and cSOR (blue) profiles of SAGD operation with 5 and 8 m thick lean zones.

3.3. Case 3: Top Gas Zone

Figure 8 displays the results for Case 3a where the top gas zone has thickness equal to 5 m. When the steam chamber reaches the top gas zone, given the constant steam injection pressure, to compensate for the loss of steam to the gas zone (where relative permeability effects do not hinder the flow of the gas into the top gas zone due to the presence of gas there), the steam rate spikes and as a consequence, so too does the iSOR. Thereafter, after the added steam has compensated for the pressure, the steam rate drops and the iSOR drops but then rises associated with the steam chamber encountering the top gas zone. Thereafter, the iSOR drops and then has a distinct change of slope. This suggests that the steam chamber has reached sufficient 'thermal momentum' so that it starts to extend laterally. Beyond this point the iSOR reaches a new minimum—this is partly caused by a top gas insulative effect that tends to lower the heat losses at the top of the reservoir versus that of losing heat to the oil sands as the steam chamber rises through the reservoir prior to it reaching the top of the formation [18,21,24,25]. Thereafter, the iSOR profile rises nearly linearly until the end of the 10 years SAGD operation as the chamber extends across the reservoir.

One noticeable difference between the top gas iSOR signal and the base case is the presence of the peak (instead of the undulations) after the chamber reaches the top of the formation as well as the delay of the point where there is a distinct change of the slope of the iSOR profile (in the top gas case, this does not align with the minimum). A difference between the top gas zone and lean zone results is the shape of the iSOR profile after the chamber reaches the top zone. There is a sharp spike in the top gas case prior to a more blunted peak with the actual maximum value tending to be at the trailing end of the profile. On the other hand, in the lean zone case, the maximum value occurs more at the leading end of the profile.

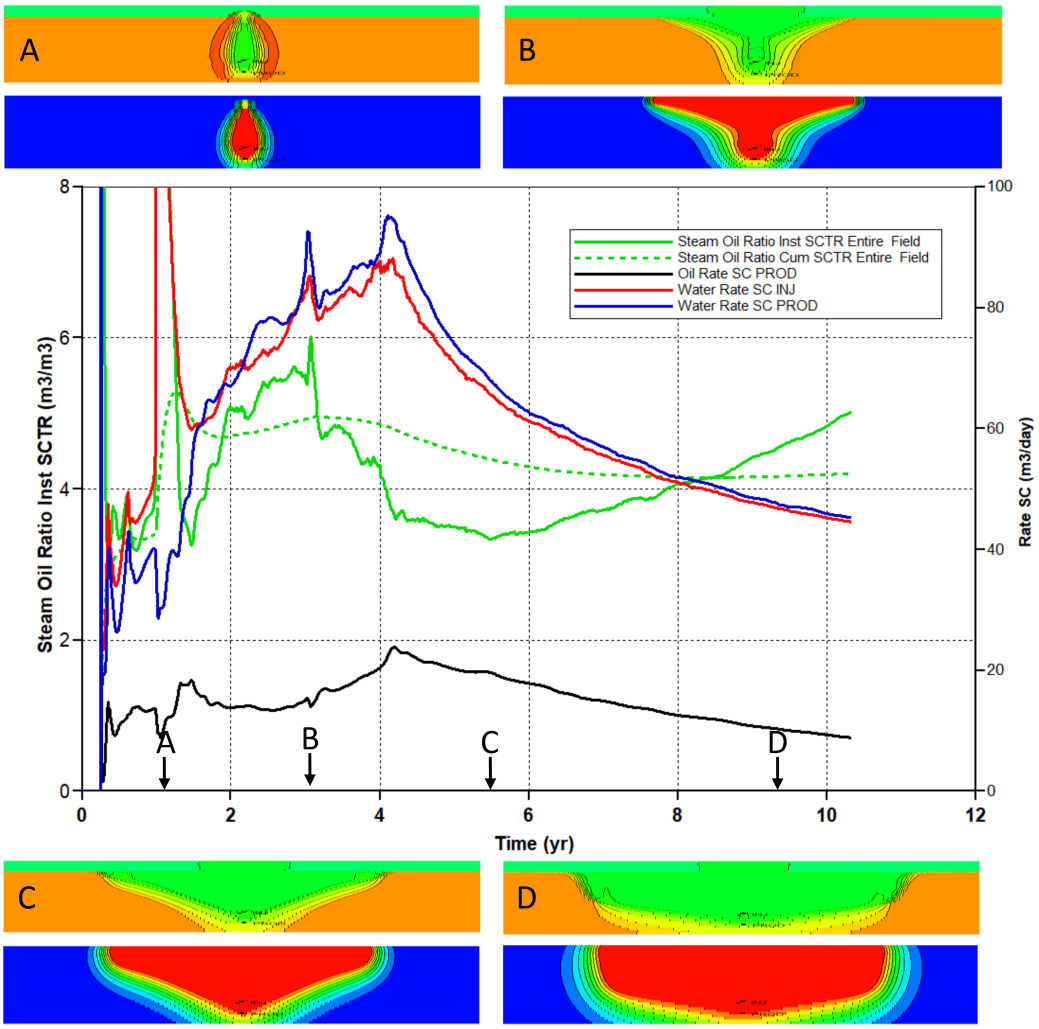

Figure 8. iSOR, cSOR, and rate profiles of SAGD operation with 5 m top gas zone at the top of the reservoir. Top images of reservoir are the oil saturation (brown = 0.75, green = ~0.22) and bottom images are the temperature profile (blue = 12 °C, red = 250 °C). The image labels (**A**–**D**) correspond to the times (**A**–**D**) in the plot.

Figure 9 displays a comparison of Cases 3a (5 m top gas zone) and 3b (8 m top gas zone). The results show that in the thicker top gas zone, the peak is higher. However, the time interval of the peak prior to the iSOR minimum (where there is a distinct change of the slope) remains about the same.

3.4. Case 4: Shale Layer

The results for Case 4a are plotted in Figure 10. A comparison of the iSOR profiles of the base case and the shale layer case demonstrates that the iSOR fluctuates when it reaches the shale layer—the reason for the fluctuations is similar to that when the steam chamber reaches the top of the formation. The condensation-drainage-replacement cycles now happen at the shale layer but since the shale layer is not too large, the iSOR profile then resumes a relatively smooth declining profile until the chamber reaches the top of the formation. The iSOR signal then varies slightly (at ~2 years of operation) as it encounters the top of the formation but the response is more muted than was the situation in the base case. This implies that the shale layer serves to dampen the iSOR response when the chamber reaches the top of the formation. After the steam chamber has reached the top of the formation and has achieved sufficient 'thermal momentum', the iSOR has a distinct change of slope (and reaches a minimum at the same time). The iSOR then rises eventually reaching a nearly constant slope which persists as the steam chamber spreads laterally across the reservoir.

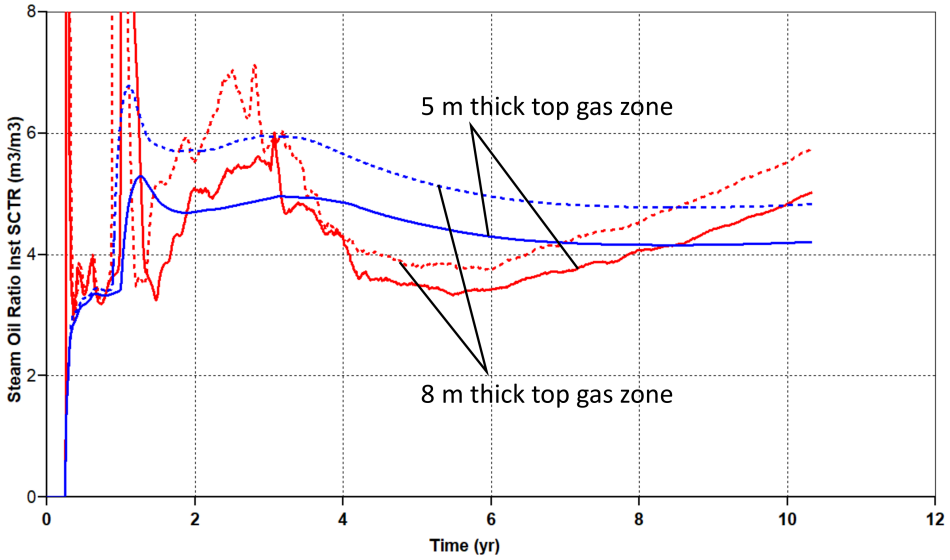

Figure 9. Comparison of iSOR (red) and cSOR (blue) profiles of SAGD operation with 5 and 8 m thick top gas zones.

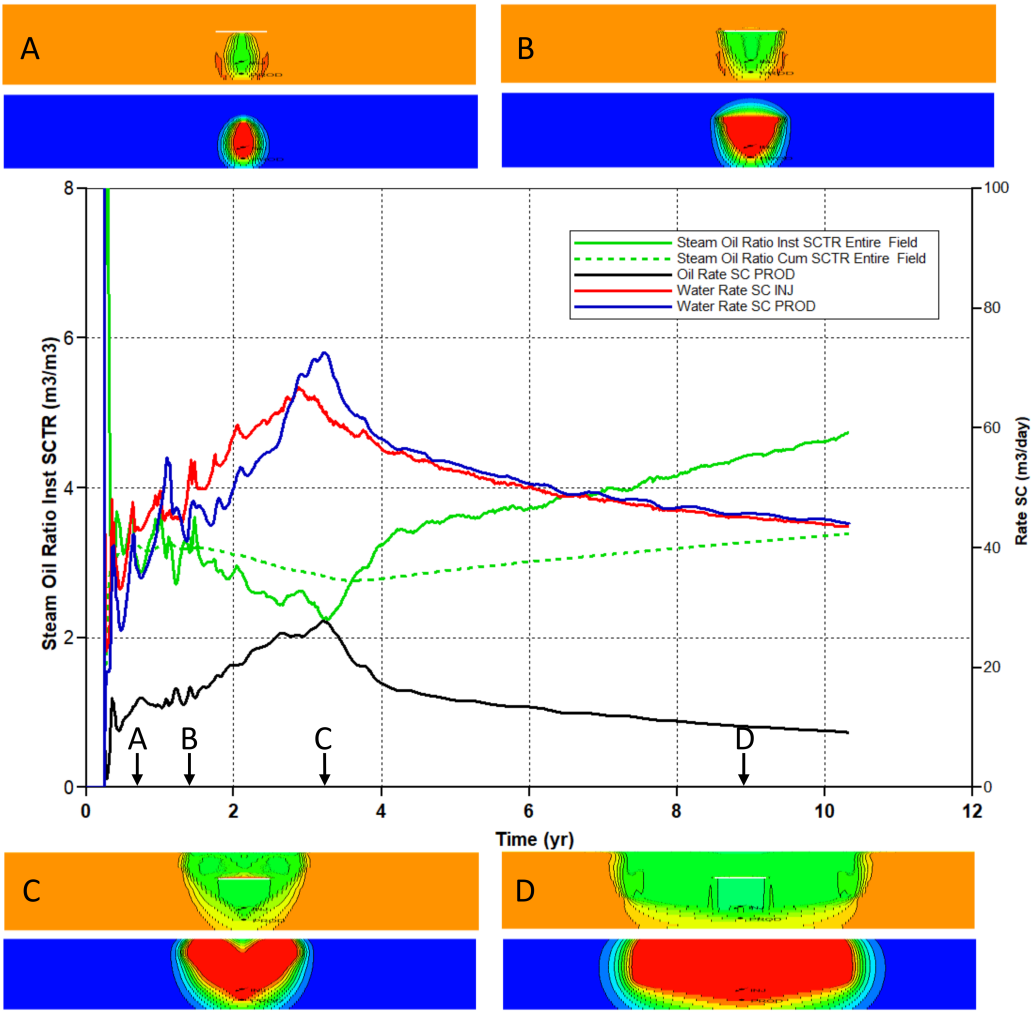

Figure 10. iSOR, cSOR, and rate profiles of SAGD operation with 20 m wide shale layer 11 m above the injection well. Top images of reservoir are the oil saturation (brown = 0.75, green = ~0.22) and bottom images are the temperature profile (blue = 12 °C, red = 250 °C). The image labels (**A**–**D**) correspond to the times (**A**–**D**) in the plot.

Figure 11 compares Cases 4a (20 m wide shale layer) and 4b (40 m wide shale layer). The 40 m wide shale layer case acts like a top of formation barrier for a period of time and so there are fluctuations of the iSOR profile. The upwards trajectory of the iSOR over the time period from 2 to 3.5 years is reflective of what an effectively thin oil sands reservoir. However, while the steam chamber spreads laterally across the shale layer, heat is transported through the shale layer to the bitumen above the shale layer. After the chamber has spread around the edges of the 40 m shale layer (after about 3.5 years of operation), the iSOR drops rapidly as the heated mobilized bitumen quickly drains to the production well and is produced. The iSOR then reaches a minimum value, with a distinct change of the slope, and then rises for the remainder of the SAGD operation.

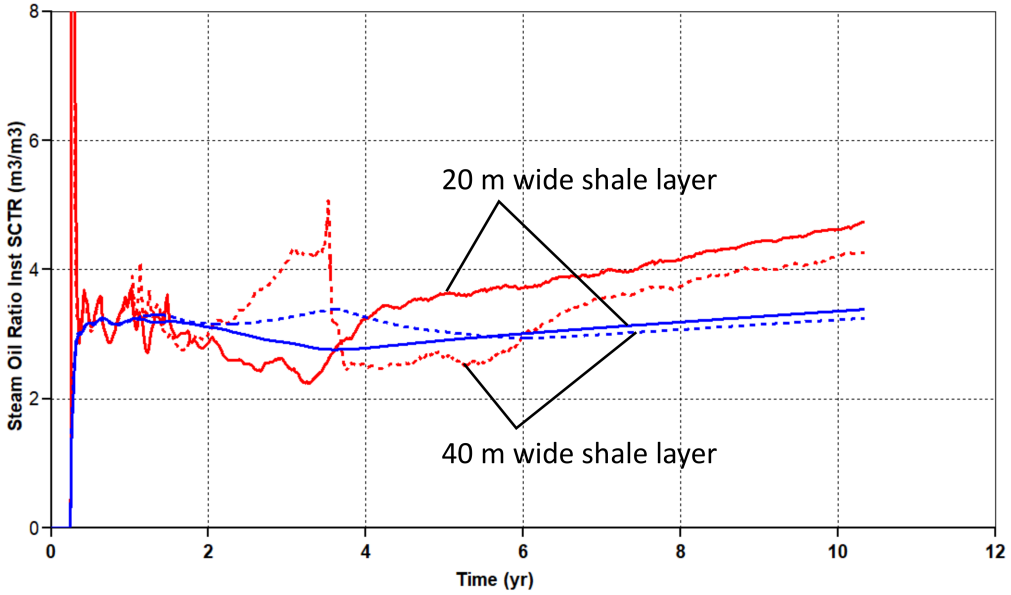

Figure 11. Comparison of iSOR (red) and cSOR (blue) profiles of SAGD operation with 20 and 40 m wide shale layers.

4. Conclusions

A study to examine how the instantaneous steam-to-oil ratio (iSOR) profile can be used to identify features of the reservoir during the steam-assisted gravity drainage (SAGD) process has been conducted. The results show that the iSOR reflects the presence of a thief zone (lean zone and top gas zone) and flow barrier (limited shale layers and extend shale layer). The results also reveal that the more extreme the feature (thicker lean of top gas zone or wide shale layer), the more pronounced is the iSOR response and the more delayed is the point where the iSOR experiences a distinct change of the slope. For the base case and lean zone, this point is coincident with the minimum iSOR whereas for the top gas cases, the minimum iSOR occurs after the point where the slope changes. Additional signals such as the production pressure should also be evaluated for response to reservoir features. For application to field operations, it is suggested that iSOR profiles should be analyzed and compared to examine the relative size of fluctuations, the delay of the point of distinct slope change, and the occurrence of a separate minimum of the iSOR profile which may suggest relative differences between reservoir features directly surrounding and above well pairs. This could be supported by using machine learning algorithms which could integrate pattern recognition involving multiple responding variables.

Author Contributions: Conceptualization, I.G. and J.W.; Data curation, J.W.; Formal analysis, J.W. and I.G.; Funding acquisition, I.G.; Investigation, J.W. and I.G.; Methodology, J.W. and I.G.; Visualization, J.W.; Writing—original draft, J.W.; Writing—review & editing, I.G. All authors have read and agreed to the published version of the manuscript.

Funding: The authors acknowledge support from the Natural Science and Engineering Research Council of Canada and the University of Calgary Canada First Research Excellence Fund program titled the Global Research Initiative in Sustainable Low Carbon Unconventional Resources.

Institutional Review Board Statement: Not applicable.

Informed Consent Statement: Not applicable.

Data Availability Statement: Not applicable.

Acknowledgments: The authors acknowledge Computer Modelling Group for the use of its thermal reservoir simulator, STARS™.

Conflicts of Interest: The authors declare no conflict of interest. The funders had no role in the design of the study; in the collection, analyses, or interpretation of data; in the writing of the manuscript, or in the decision to publish the results.

References

1. Butler, R.M. Steam-Assisted Gravity Drainage: Concept, Development, Performance and Future. *SPE Repr. Ser.* **2008**, *61*, 44–50. [CrossRef]
2. Butler, R.M. *Thermal Recovery of Oil and Bitumen*; Prentice-Hall Inc.: Upper Saddle River, NJ, USA, 1991; ISBN 9780139149535.
3. Gates, I.D. *Basic Reservoir Engineering*; Kendall Hunt Publishing Company: Dubuque, IA, USA, 2011.
4. Zhou, S.; Huang, H.; Liu, Y. Biodegradation and origin of oil sands in the western Canada sedimentary basin. *Pet. Sci.* **2008**, *5*, 87–94. [CrossRef]
5. Khan, M.A.B.; Mehrotra, A.K.; Svrcek, W.Y. Viscosity Models for Gas-Free Athabasca Bitumen. *J. Can. Pet. Technol.* **1984**, *23*, 47–53. [CrossRef]
6. Gates, I.D.; Larter, S.R. Energy efficiency and emissions intensity of SAGD. *Fuel* **2014**, *115*, 706–713. [CrossRef]
7. Millington, D. *Study No. 183: Canadian Oil Sands Supply Projects Development Costs (2019–2039)*; Canadian Energy Research Institute: Calgary, AB, Canada, 2019; p. 53.
8. Gates, I.D.; Chakrabarty, N. Optimization of Steam-Assisted Gravity Drainage (SAGD) in Ideal McMurray Reservoir. *J. Can. Pet. Technol.* **2006**, *45*, 54–62. [CrossRef]
9. Gates, I.D.; Kenny, J.; Hernandez-Hdez, I.L.; Bunio, G.L. Steam Injection Strategy and Energetics of Steam-Assisted Gravity Drainage. *SPE Reserv. Eval. Eng.* **2007**, *10*, 19–34. [CrossRef]
10. Bao, Y. On Steam Based Recovery Process Design. Ph.D. Thesis, University of Calgary, Calgary, AB, Canada, 2015.
11. Guo, T.; Wang, J.; Gates, I.D. Pad-scale control improves SAGD performance. *Petroleum* **2018**, *4*, 318–328. [CrossRef]
12. Su, Y.; Wang, J.; Gates, I.D. SAGD Well Orientation in Point Bar Oil Sands Deposit Affects Performance. *Eng. Geol.* **2013**, *157*, 79–92. [CrossRef]
13. Su, Y.; Wang, J.; Gates, I.D. Orientation of a Pad of SAGD Well Pairs in an Athabasca Point Bar Deposit Affects Performance. *Mar. Pet. Geol.* **2014**, *54*, 37–46. [CrossRef]
14. Su, Y.; Wang, J.; Gates, I.D. SAGD Pad Performance in a Point Bar Deposit with a Thick Sandy Base. *J. Pet. Sci. Eng.* **2017**, *154*, 442–456. [CrossRef]
15. Wei, W.; Gates, I.D. On the Relationship between Completion Design, Reservoir Characteristics, and Steam Conformance Achieved in Steam-Based Recovery Processes Such as SAGD. *SPE-DOE Improv. Oil Recovery Symp. Proc.* **2010**, *1*, 460–476.
16. Lastiwka, M.; Bailey, C.; James, B.; Zhu, D. A practical approach to the use and design of flow control devices in SAGD. In Proceedings of the Society of Petroleum Engineers-SPE Canada Heavy Oil Technical Conference, Calgary, AB, Canada, 7–9 June 2017; pp. 777–789. [CrossRef]
17. Alturki, A.A.; Gates, I.D.; Maini, B.B. Co-injection of non-condensable gas improves ES-SAGD performance in shallow oil sands reservoirs with a small top water zone. In Proceedings of the Society of Petroleum Engineers-Canadian Unconventional Resources and International Petroleum Conference, Calgary, AB, Canada, 19–21 October 2010.
18. Austin-Adigio, M.; Gates, I.D. Non-Condensable Gas Co-Injection with Steam for Oil Sands Recovery. *Energy* **2019**, *179*, 736–746. [CrossRef]
19. Gates, I.D.; Leskiw, C. Impact of Steam Trap Control on Performance of Steam-Assisted Gravity Drainage. *J. Pet. Sci. Eng.* **2010**, *75*, 215–222. [CrossRef]
20. Edmunds, N.; Chhina, H. Economic Optimum Operating Pressure for SAGD Projects in Alberta. *J. Can. Pet. Technol.* **2001**, *40*, 13–17. [CrossRef]
21. Pinto, H.; Wang, X.; Gates, I.D. Insights on Heat Transfer at the Top of Steam Chambers in SAGD. *J. Heat Transf.* **2017**, *139*, 041801. [CrossRef]
22. Gotawala, D.R.; Gates, I.D. On the Impact of Permeability Heterogeneity on SAGD Steam Chamber Growth. *Nat. Resour. Res.* **2010**, *19*, 151–164. [CrossRef]

23. Vinsome, P.K.W.; Westerveld, J. A Simple Method for Predicting Cap and Base Rock Heat Losses in Thermal Reservoir Simulators. *J. Can. Pet. Technol.* **1980**, *19*, 87–90. [CrossRef]
24. *CMG STARS™ User's Manual*; Version 2019; Computer Modelling Group Ltd.: Calgary, AB, Canada, 2019.
25. Yuan, J.Y.; Chen, J.; Pierce, G.; Wichar, B.; Golbeck, H.; Wang, X.; Beaulieu, G.; Cameron, S. Noncondensable Gas Distribution in SAGD Chambers. *J. Can. Pet. Technol.* **2011**, *50*, 11–20. [CrossRef]